Article:

Davies, A, Gréselle, B, Hunter, SJ orcid.org/0000-0002-4593-6238 et al. (6 more authors) (2020) Assessing the impact of aquifer-eustasy on short-term Cretaceous sea-level. Cretaceous Research, 112. 104445. ISSN 0195-6671

https://doi.org/10.1016/j.cretres.2020.104445

Assessing the Impact of Aquifer-Eustasy on Short-Term Cretaceous Sea Level

Andrew Davies[1*] Benjamin Gréselle[1], Stephen Hunter[2], Graham Baines[1], Chris Robson[1], Alan Haywood[2], David C. Ray[1], Michael D. Simmons[1], Frans S.P. van Buchem[1]

[1]*Halliburton, 97 Jubilee Avenue, Milton Park, Abingdon, UK*

[2]*University of Leeds, School of Earth and Environment, Leeds, UK*

*corresponding author: andrew.davies@halliburton.com

Abstract

The origin of moderate magnitude (tens of metres), short-term Cretaceous eustatic cycles remains enigmatic. The historical view of ubiquitous Cretaceous warmth casts doubt on the presence of significant terrestrial ice caps and the role of glacio-eustasy. As such, aquifer-eustasy is increasingly advocated as the primary driver of Cretaceous short-term sea-level change. Here, we analyse the role of aquifer-eustasy in driving Cretaceous short-term cycles by assessing the spatio-temporal pattern of aridity and humidity under differing CO_2 forcing in new climate simulations for the Valanginian, Turonian, and Maastrichtian. Elevated CO_2 forcing acts to increase the spatial extent of fully arid land areas, while resulting in only a marginal expansion of fully humid zones. Consequently, the greatest aquifer charge is more likely during lower CO_2/cooler intervals, indicating that aquifer-eustasy works in phase with both glacio- and thermo-eustasy in contrast to the current aquifer-eustasy paradigm. Modern data indicate that climate is a primary control on water table depth. Using this constraint, the hydrological response in our Cretaceous simulations to large changes in atmospheric CO_2 are insufficient to generate reported eustatic magnitudes. Our most likely aquifer-eustasy estimates are decimetre scale. Even using optimistic values for the impact of lakes and assuming the water table depth was reduced from the modern average to 0 m globally, the total aquifer-eustasy response remains smaller than 5 m. Our results indicate that glacio-

eustasy was the most likely driver of Cretaceous short-term cycles, consistent with a growing body of evidence that challenges the ubiquitously warm Cretaceous notion.

1. Introduction

Although short-term (<3 million years) sea-level cycles are well documented in the Cretaceous (Immenhauser, 2005; Miller et al., 2005a, 2005b; Voigt et al., 2006), their origins have remained a subject of debate. However, there is growing evidence that many short-term cycles are synchronous (Gale et al., 2002; Wilmsen and Nagm, 2013; Wendler et al., 2014) and eustatic in nature (Miller et al., 2005a). This has been supported by the recent collation and analysis of approximately 800 published estimates of the magnitude of Cretaceous short-term sea-level change, which demonstrates a stage-level synchronicity in the magnitude of sea-level change as well as longer-term magnitude trends (Ray et al., 2019). In combination, this information suggests that a significant proportion of published sea-level estimates reflect globally synchronous sea-level changes (eustasy), and that these eustatic events occur at frequencies that can be best accounted for by orbitally influenced climatic processes (Boulila et al., 2011; Sames et al., 2016).

The climatic drivers of short-term cyclic eustasy are limited to density-driven changes in the volume of the oceans (thermo-eustasy) and processes that influence the exchange of water between the ocean and terrestrial stores, such as aquifers (aquifer-eustasy) or ice caps (glacio-eustasy) (Sames et al., 2016). An important starting point for identifying the drivers of Cretaceous short-term eustasy is an assessment of the upper magnitudes of eustatic cycles through time. This has been conducted for the entire Cretaceous (Ray et al., 2019) and demonstrates that short-term cycles of significant magnitude (>40 m) occur during the Valanginian, Aptian, Albian, and Maastrichtian, slight magnitude cycles (<10 m) are restricted to the Berriasian, and moderate cycles (10 to 40 m) characterise the remaining stages of the Cretaceous.

The temporal changes in Cretaceous magnitudes documented by Ray et al. (2019) can be compared to the upper magnitude limits of thermo- and glacio-eustasy, which are distinct and well established at 10 m and more than 200 m, respectively. However, the upper limit of aquifer-eustasy is more poorly constrained (Ray et al., 2019). Aquifer-eustasy relies on short-term fluctuations in precipitation patterns that result in spatiotemporal shifts in the areal extent of arid and humid zones (Wagreich et al., 2020). This results in the differential charge of available aquifers, affecting the net water balance between the continents and oceans (Wendler et al., 2016). Observations of long-term, temperature-driven shrinkage/expansion of the intertropical convergence zone humid belt provides support to the active role of aquifer-eustasy in the Cretaceous (Hasegawa et al., 2012; Hay and Floegel, 2012). However, estimates of aquifer-eustasy magnitudes range widely from 8 m (Jacobs and Sahagian, 1993) to 50 m (Hay and Leslie, 1990) to as much as 100 m (Haq and Huber, 2017). Of these estimates, those provided by Hay and Leslie (1990) are the most frequently citied, although their estimate of a 50 m aquifer-eustasy limit requires the alternate filling and emptying of all available present-day aquifers and might therefore be unrealistic. Nonetheless, a consensus has begun to form around magnitudes of 10 to 40 m being obtainable during the Cretaceous by invoking larger aquifer volumes and a more vigorous hydrological cycle (Wendler et al., 2016; Wendler and Wendler, 2016).

A further complicating factor in establishing the drivers of short-term Cretaceous eustasy relates to the climatic controls upon thermo- and glacio-eustasy. For example, the temperature of the entire volume of water in the global ocean would need to increase by ~10°C to generate a 6 m eustatic rise (Sundquist, 1990). Therefore, a 10 m short-term, thermo-eustatic cycle would require a temperature fluctuation equivalent to the early Eocene Climate Optimum to the present (Cramer et al., 2011). This is inconsistent with planktonic and benthic climate proxy records (Huber et al., 2002; Cramer et al., 2011; O'Brien et al., 2017). Climate proxies also document that the Cretaceous experienced substantially warmer climates than present

(Jenkyns et al., 2004; Vickers et al., 2019), supported by the occurrence of forests (e.g. Bowman et al., 2014) and ectothermic reptile species (e.g. Vandermark et al., 2007) at high latitudes. This poses significant challenges to the role of glacio-eustasy, resulting in aquifer-eustasy being increasingly advocated as the primary driver of Cretaceous short-term eustatic cycles (Föllmi, 2012; Sames et al., 2016; Wendler et al., 2016; Wendler and Wendler, 2016; Laurin et al., 2019; Sames et al., 2020). However, the assumption of a 40 m upper magnitude limit for aquifer-eustasy poses a challenge to the role of aquifer-eustasy in that approximately 50% of the Cretaceous is associated with larger magnitude cycles (Ray et al. 2019). Furthermore, Ray et al. (2019) demonstrated that the largest magnitude (up to 65 m), short-term sea-level variations occur during the coolest stages of the Cretaceous, which is inconsistent with the aquifer-eustasy paradigm (Wendler et al., 2016), leading Ray et al. (2019) to the conclusion that glacio-eustasy was the fundamental driver of short-term eustatic cycles. This view is supported by a range of data that challenge the notion that the Cretaceous was ubiquitously warm. Geochemical proxy estimates indicate evident long-term trends with distinct cooler conditions in the Valanginian-Barremian, Late Aptian, and Maastrichtian (e.g., O'Brien et al., 2017). Evidence for cold high-latitude conditions have been reported during these times (Davies et al., 2009; Bowman et al., 2013; Grasby et al., 2017), which, when combined with geochemical (Bornemann et al., 2008) and sequence stratigraphic insights (Kominz et al., 2008; Maurer et al., 2013; Uličný et al., 2014), makes the reported presence of polar ice sheets (Alley et al., 2019) plausible. This possibility is further supported by the downward revision of Cretaceous atmospheric CO_2 concentrations (e.g., Breecker et al., 2010).

Here, we explore the climatic controls and likely magnitude limits of aquifer-eustasy for three time intervals characterised by differing short-term magnitudes (Ray et al., 2019) (Figure 1). We focus on the Turonian, when short-term magnitudes were modest (~30 m) and available geochemical proxies indicate peak Cretaceous warmth was reached (O'Brien et al., 2017), and the Valanginian and Maastrichtian, when short-term magnitudes were more significant

(~65 and ~50 m, respectively) and cooler climatic conditions prevailed. We use new climate simulations using the Hadley Centre Coupled Climate Model Version 3 (HadCM3L) to assess the spatio-temporal trends in precipitation and resulting arid and humid zones under differing CO_2 forcing to determine the likely impact on aquifer storage. The area of deserts in each simulation is compared to the present to assess whether the enhanced hydrological cycle during the Cretaceous could have resulted in enhanced aquifer storage. Modern water table data are used to quantify the likely aquifer-eustasy response.

2. Methods

2.1 Climate Simulations

The HadCM3L general circulation model (Gordon et al., 2000; Pope et al., 2000) was used to generate new simulations for the Valanginian, Turonian, and Maastrichtian. We incorporated the land surface scheme MOSES 2.1 (Essery et al., 2003) and the TRIFFID dynamic global vegetation model (Cox, 2001). The tectonic configuration, gross depositional environments, and resulting paleo digital elevation models (PDEM) that underpin this study were created by Halliburton Neftex® Insights using a modified version of the approach of Vérard et al. (2015) to include a wider range of input data. The PDEM, land-sea mask, and lake fields were regridded to model resolution using an area-weighted algorithm. Model-specific smoothing was applied to the bathymetry, and hand edits were applied where the land-sea mask was unsatisfactory. A model resolution river drainage model was generated that is internally consistent with the PDEM and known river outlets.

Three simulations were conducted for each time slice with differing atmospheric CO_2 concentrations to explore the potential impact of short-term climate variations on the spatio-temporal trends in precipitation and resulting arid and humid zones. A compilation of available proxy estimates for atmospheric CO_2 concentrations was generated for the three time periods (refer to the supplementary information), and low, medium, and high atmospheric CO_2

concentrations were prescribed for each simulation (Table 1). Other atmospheric constituents were held at preindustrial levels.

Annual precipitation data over land were extracted from the time-averaged simulation results, and data were binned by latitude using the model grid cells. Zonal mean, maximum, and minimum values were obtained. To further assess the spatial changes in precipitation and evaporation patterns, climate zones were identified using the Köppen-Geiger climate classification scheme (Kottek et al., 2006) for each simulation and the total area of each class calculated.

To test the validity of the simulations, a database of proxies indicating land aridity (calcretes and evaporites) and humidity (bauxites, coals, crocodiles, laterites, and palms) was collated from Boucot et al. (2013). Although Boucot et al. (2013) do not use crocodiles and palms as exclusive indicators of humid climates, their work demonstrates that they do not generally co-occur with proxies for aridity. This is supported by data demonstrating that modern palms are far more common in non-arid zones (Reichgelt et al., 2018) and that the geographic pattern of decline among fossil crocodilians matches patterns of aridification in Africa and South America (Mannion et al., 2015). Because the time slices analysed by Boucot et al. (2013) are much broader than those used here, any data that could be determined not to be Valanginian, Turonian, or Maastrichtian in age were removed. Information on aeolian deposits was collated from Argentina (Buatois and Echevarría, 2019), Brazil (Scherer, 2002; Dal' Bó et al., 2009), China (Hasegawa et al., 2012), France (Kindler and Davaud, 2001), Namibia (Mountney et al., 1998), Mongolia, and Thailand (Hasegawa et al., 2012) to bolster the arid proxy control. Because of the poor chronostratigraphic control on many of the proxies, a temporal confidence was applied to differentiate data that could be definitively tied to the stage of interest from covering multiple stages. In total, this resulted in 109 proxies for the Valanginian, 68 for the Turonian, and 110 for the Maastrichtian.

2.2 Water Tables

To allow the eustatic impact of changes in land surface hydrology to be quantified, we utilised a global modern water table depth dataset from Fan et al. (2017). A statistical analysis of the total dataset was conducted along with an analysis of the fully arid and non-arid land areas. Modern land area types were identified using the Köppen-Geiger map for 1976-2000 from Rubel and Kottek (2010).

3. Results

Results from the simulations demonstrate a close match with the available proxies for the different time slices (Figure 2). The Köppen-Geiger predictions also demonstrate a good agreement with the broader chronological synthesis of Boucot et al. (2013), suggesting that the simulations represent a robust estimation of the studied time periods. Analysis of the global mean precipitation in the nine climate simulations demonstrates that the higher CO_2 forcing generally results in elevated global precipitation indicative of an enhanced hydrological cycle (Table 2). The only exception is the Valanginian where global mean precipitation increases from the low to middle CO_2 forcing but declines in the highest CO_2 forcing.

However, as might be expected, the elevated precipitation as a consequence of increased CO_2 forcing is not evenly distributed but rather is concentrated in equatorial humid belts and at mid to high latitudes in humid to semi-humid belts (Figure 3). Precipitation in tropical arid belts either remains constant or decreases with elevated CO_2 forcing (Figure 3). To explore the spatial impact CO_2 forcing has on precipitation, a map was created to demonstrate the difference in precipitation between the simulations with the highest and lowest atmospheric CO_2 concentrations for each time slice (Figure 4). The spatial response is complex, but the general increase in precipitation observed in the zonal median analysis in mid-high latitudes and equatorial regions in response to greater CO_2 forcing (Figure 3) is apparent. A clear trend is also evident when the fully arid land areas on the lowest CO_2 simulations are overlain with precipitation in these areas, demonstrating little change with CO_2 forcing. Additionally, adjacent areas exhibit a clear trend of decreasing precipitation with increased CO_2 forcing. This reduction in precipitation explains the expansion of the fully arid land area with increasing CO_2 forcing, as predicted from the Köppen-Geiger classification for the different time slices (Figure 2). An analysis of the area of fully arid land demonstrates a consistent expansion with higher atmospheric CO_2 concentrations (Figure 5). Conversely, the geographical area of fully humid zones is generally at its greatest under lower CO_2 forcing, and the variance between simulations is reduced (Figure 5).

Longer-term trends are also apparent from this study. The analysis of both the mean global precipitation (Table 2) and the spatial extent of the fully arid and fully humid land areas (Figure 5) demonstrates that the Valanginian was considerably drier than the Turonian or Maastrichtian. This is likely a reflection of the greater continentality of the Valanginian when the break-up of Pangea was in an earlier stage and multiple epicontinental seaways and oceans characterising the Turonian and Maastrichtian had yet to form, including the South Atlantic (Granot and Dyment, 2015), Western Interior Seaway (Miall and Catuneanu, 2019), Labrador-Baffin Bay (Dickie et al., 2011), Turgay Seaway (Kontorovich et al., 2014), and the South Australian Bight (Totterdell et al., 2001).

4. Discussion

4.1 Aquifer-Eustasy Magnitudes

To assess the eustatic impact of the spatial shifts in precipitation predicted by our simulations, it is first necessary to understand how climate impacts aquifer capacity. Modern data (Fan et al., 2013, 2017) indicate that at a regional scale, climate is the primary control on water tables, which are generally shallow (aquifers near full) in fully humid and partially humid areas and are only deep in fully arid zones and mountainous regions (Figure 6). Any changes in the spatial extent of the fully arid land area is therefore likely to have the most significant impact on aquifer storage and hence global sea level. The fully arid land area between the simulations with the highest and lowest CO_2 forcing differ by 15.6, 9.6, and 8.4 million km^2 for the Valanginian, Turonian, and Maastrichtian, respectively (Table 3).

Next, it is necessary to determine the likely impact the changes in fully arid land areas had on water column height. The depth of the water table in modern fully arid zones is highly variable, ranging from 0 to 986.8 m deep (Fan et al., 2013, 2017). However, the data are highly skewed, with 90% of the arid land area having a water table depth of 79.07 m or shallower. The geometric mean water table depth in fully arid areas is 18.90 m with a median value of 25.87 m (for the full statistics see the supplementary information). We use the median value and make an assumption that the water table depth rises to the non-arid median water table depth of 11.20 m. The non-arid water table depths are also highly skewed, with 90% of the land area having depth of 62.91 m or shallower, and a geometric mean value of 4.66 m (for the full statistics see the supplementary information). It has been suggested that Cretaceous artesian basins were composed of a higher percentage of younger, more porous sediments compared to the present currently (Hay and Leslie, 1990); therefore, we assume an optimistic porosity of 30%. Given these assumptions, we can estimate the change in the volume of water stored in the aquifers because of the changes in the fully arid land area between the high and low CO_2 simulations for each time period (Table 3). To assess the sea-level impact of any given volume of water, it is necessary to know the total ocean area. Our reconstructions indicate this is 184.4, 136.7, and 135.8 million km^2 for the Valanginian, Turonian, and Maastrichtian, respectively. This allows us to estimate that 0.325, 0.373, and 0.374 million km^3 of water is necessary to generate a 1 m eustatic change for the Valanginian, Turonian, and Maastrichtian, respectively (refer to the supplementary information).

With this information, it is possible to determine a most likely impact of the simulated changes in the fully arid land area (Table 3, scenario 1) were 0.21, 0.11, and 0.10 m for the Valanginian, Turonian, and Maastrichtian, respectively (for upper and lower estimates calculated using P10 and P90 values see the supplementary information). These estimates are several orders of magnitude different to the most robust estimates of short-term eustatic magnitudes of 65, 30, and 50 m for the Valanginian, Turonian, and Maastrichtian, respectively (Ray et al., 2019), posing a challenge to the role of aquifer-eustasy in controlling moderate amplitude short-term sea-level cycles in the Cretaceous. In addition, although Cretaceous atmospheric CO_2 estimates exhibit a high degree of variability (e.g. Wang et al., 2014; also refer to the supplementary information), the values used in our simulations (Table 1) likely represent endmember scenarios and, in general, overestimate the magnitude of short-term variability in atmospheric concentrations. During the Cenomanian-Turonian, Oceanic Anoxic Event 2, atmospheric CO_2 concentrations increased rapidly as a result of elevated rates of volcanic degassing associated with high seafloor spreading rates and initial emplacement of the Caribbean large igneous plateau (Jarvis et al., 2011). Following this, atmospheric CO_2 concentrations sharply reversed in response to the onset of widespread black shale deposition (Jarvis et al., 2011). However, even during this extreme event, it appears unlikely that atmospheric CO_2 concentrations varied by the magnitudes used in our simulations (e.g., Barclay et al., 2010; Jarvis et al., 2011).

Although we have concentrated so far on the impact of the changes in a fully arid land area, it is worth exploring the possible impacts of other scenarios. Although not supported by our simulations, if it were possible to fill the median aquifer space in the total arid area of the medium CO_2 simulations to the non-arid area median, the eustatic response would still be only 0.78, 0.48, and 0.44 m for the Valanginian, Turonian, and Maastrichtian, respectively (Table 3, scenario 2. For upper and lower estimates see the supplementary information). Although humid and semi-humid regions currently have little aquifer space available (Fan et al., 2017, 2013), the additional rainfall in these area might have impacted the water table depth. Because of the difficulty in assessing the water table impact of the additional precipitation in humid areas, we can take an extremely optimistic approach and use the median global water table depth (neglecting Antarctica and Greenland where data are unavailable) of 16.70 m (Fan et al., 2017) and assume that this was reduced to zero over the global land surface area, including fully arid zones. This very unlikely scenario generates a eustatic response of 2.84, 1.83, and 1.82 m for the Valanginian, Turonian, and Maastrichtian, respectively (Table 3, scenario 3. For upper and lower estimates see the supplementary information). What global change in the water table depth would be necessary to explain the reported short-term eustatic cycles of 65, 30, and 50 m for the Valanginian, Turonian, and Maastrichtian (Ray et al., 2019)? Using the preceding logic, an average shift in global aquifer depth of 383, 273, and 459 m would be necessary for the Valanginian, Turonian, and Maastrichtian (see the supplementary information). Given that the global median water table depth in the modern world is 16.70 m (Fan et al., 2017) and only 0.12% of the modern land surface has a water table deeper than 273m, such magnitudes appear unrealistic.

Aquifers are not the only medium that can influence the exchange of water between the ocean and terrestrial stores. It has been suggested that lakes and rivers could also have a role in terrestrial water storage resulting from spatio-temporal changes in precipitation (Föllmi, 2012). Whilst the exact impact of lakes and rivers needs additional study, it has been regarded as negligible (Sames et al., 2016). By assessing the volume of the 10 largest modern internally draining basins that are dry, it is possible to generate a eustatic response of 2.09 m if all these become full to spill (Jacobs and Sahagian, 1993). However, given the fact that the broad arid areas are persistent in our simulations under different CO_2 forcing, this appears unlikely. Additional research is necessary to assess whether changes in orbital configuration might impact this conclusion and the changes in fully arid land area more generally. However, even if lakes were able to contribute to a ~2 m eustatic response and different orbital parameters acted to completely move arid areas into ocean basins so that all land areas became humid and the water table depth was reduced from the modern median of 16.70 to 0 m globally, the largest likely total aquifer-eustasy response remains smaller than 5 m (Figure 7).

4.2. Aquifer-Eustasy Phase

In the established aquifer-eustasy paradigm, an enhanced hydrological cycle during warmer time intervals results in a shift in the net water balance from the ocean to the continents, causing global sea levels to fall (Wendler and Wendler, 2016). Conversely, during cooler intervals characterised by decreased precipitation on land, aquifers receive less charge, and there is a net exchange of water from land to ocean causing global sea levels to rise.. Therefore, in the current paradigm, aquifer- and glacio/thermo-eustasy have opposing sea-level impacts for a given change, preventing them from working in tandem (Ray et al., 2019; Sames et al., 2020). Accordingly, climatic warming increases sea level by thermo- and glacio-eustasy; however, in the current paradigm, an enhanced hydrological cycle would transfer water from the oceans to aquifers, causing a eustatic fall (Wendler and Wendler, 2016).

Our results demonstrate that the current aquifer-eustasy paradigm might be incorrect, in that the simulations demonstrate a consistent trend for increasing fully arid land surface area with higher CO_2 forcing (Figure 5). Furthermore, the results are consistent with an observed increase in land aridity since 1948 (Huang et al., 2016) and with the predicted continued expansion of arid zones as a result of anthropogenic CO_2 forcing (Berg et al., 2016). Therefore, during warmer conditions, aquifers are likely to hold less water globally, and there is a net transfer of water to the ocean resulting in a eustatic rise. Consequently, our results indicate that aquifer- and glacio-eustasy work in phase and they work in concert with thermo-eustasy. Moreover, if correct, such a finding might explain modest magnitude sea-level changes as a combination of drivers with small eustatic contributions of thermo- and aquifer-eustasy supplemented by glacio-eustasy in response to the waxing and waning of small and possibly ephemeral ice caps (Figure 7).

4.3. Implications on the Origin of Cretaceous Short-Term Eustatic Cycles

Support for the current aquifer eustasy paradigm has been derived from the Songliao Basin, China, where the Turonian eustatic model of Haq (2014) appears to be out of phase with lacustrine water level changes (Wagreich et al., 2014). Further, marine transgressions in the Turonian Chalk of the UK appear to be associated with cooling and regressions with warming (Wendler and Wendler, 2016). Although intriguing, such scant evidence does not permit definite statements on the role of aquifer eustasy on Cretaceous short-term eustasy. Significant challenges are associated with establishing a sequence stratigraphic framework in pelagic successions and the conclusions of Wendler and Wendler (2016) are in direct opposition to those of other workers who analysed the same chalk succession (e.g. Jarvis et al., 2015). Unfortunately direct comparisons between paleotemperature and systems tracts during the Cretaceous are relatively rare, but a number of studies exist which demonstrate transgressions are associated with warming and regressions with cooling (e.g. Mutterlose et al., 2009; Cramer et al., 2011). Additionally, it has been noted that during the Cretaceous, the magnitude of short-term eustatic cycles correlates with broad temperature trends (Ray et al., 2019). Comparison of long term Cretaceous trends illustrate that the coolest time intervals are associated with the largest short-term magnitudes, whilst the warmest are associated with the smallest magnitudes. As the current aquifer-eustasy paradigm invokes an inverse relationship between aquifer- and glacio-eustasy (Sames et al., 2020), this observation argues against aquifer-eustasy being the primary driver of Cretaceous cycles. In conjunction with this, the magnitudes of sea-level change during the cooler intervals were in excess of what could be considered as the plausible 40 m upper magnitude limit of aquifer-eustasy. From these observations, Ray et al. (2019) concluded that during the Cretaceous, glacio-eustasy dominates short-term eustatic change with only the Berriasian, Turonian, and Coniacian having equivocal driving mechanisms.

Our estimates of the magnitude of aquifer-eustasy for the Valanginian, Turonian, and Maastrichtian demonstrate that this process is unlikely to have caused the reported magnitudes (Ray et al., 2019), even during the warmest periods of the Cretaceous (Figure 7). Therefore, this study supports a growing view that glacio-eustasy was a dominant eustatic mechanism during much of the Cretaceous, mediated by changes in volume of relatively small polar ice caps and episodic cold spells (Miller et al., 2005b; Galeotti et al., 2009; Koch and Brenner, 2009; Gréselle and Pittet, 2010; Maurer et al., 2013) alongside the in-phase contributions of thermo- and aquifer-eustasy. Despite ongoing perceptions in much of the geological community that the Cretaceous was dominated by persistent warm climates (e.g., Hay et al., 2019), this view is increasingly challenged by climate modelling studies (e.g., Ladant and Donnadieu, 2016; Niezgodzki et al., 2019), sedimentological evidence (Macquaker and Keller, 2005; Davies et al., 2009; Alley et al., 2019; Vickers et al., 2019), estimates of the magnitude of short-term eustatic cycles (Lin et al., 2019; Ray et al., 2019)and changes in fossil assemblages (Mutterlose et al., 2009; Bowman et al., 2013; McAnena et al., 2013). However, the role of glacio-eustasy is in contrast with geochemical proxy evidence (e.g. TEX_{86}, $\delta^{18}O$, Mg/Ca), which generally implies that the Cretaceous was too warm for the presence of ice caps. This is well illustrated by the disparity between Maastrichtian TEX_{86} estimates of mean annual sea surface temperature of ~15°C for the Arctic Ocean (Jenkyns et al., 2004) with contemporaneous evidence for seasonal sea ice (Davies et al., 2009). Whilst this is a challenge that deserves additional future research, it is possible that these discrepancies might relate to calibration issues (Ho and Laepple, 2016; Bernard et al., 2017) and the presence of a seasonal bias in many geochemical proxy temperature estimates, particularly at high latitudes (Hollis et al., 2012; Davies et al., 2019).

5. Conclusions

We have used a range of climate simulations for the Valanginian, Turonian, and Maastrichtian to assess the assumptions behind the role of aquifer-eustasy in the Cretaceous. The Köppen-Geiger zones resulting from the simulations demonstrate good agreement with available proxies for humidity and aridity on land, suggesting they represent a robust estimation of the studied time periods. The simulations demonstrate that higher CO_2 forcing generally results in an enhanced hydrological cycle with elevated global precipitation over land. However, the increase in precipitation is concentrated in equatorial and mid-latitude areas that are generally humid or semi-humid under different CO_2 forcings. As a result, there are only limited changes in the spatial extent of arid and humid zones in response to large changes in CO_2 forcing, with geodynamic processes and continental configuration controlling long-term climatic trends. The fully arid land area between the simulations with the highest and lowest CO_2 forcing differ by 15.6, 9.6, and 8.4 million km^2 for the Valanginian, Turonian, and Maastrichtian, respectively.

In our most likely scenario the changes in fully arid land areas in our simulations would generate eustatic responses of 0.21, 0.11, and 0.10 m for the Valanginian, Turonian, and Maastrichtian, respectively, assuming a change in water table depth from the modern fully arid area median of 25.87 m to the non-arid area median of 11.20 m (Fan et al., 2017). Even if it were possible to change the water table depth in the total arid area of the medium CO_2 simulations to that of the median non-arid area, the eustatic response would be only 0.78, 0.48, and 0.44 m for the Valanginian, Turonian, and Maastrichtian, respectively. Although humid and semi-humid regions have little aquifer space available, the additional rainfall in these areas might have impacted the water table depth. In our most optimistic scenario using the modern median global water table depth of 16.70 m (Fan et al., 2017), and assuming this was reduced to zero over the total global land surface area, the eustatic response could reach 2.84, 1.83, and 1.82 m for the Valanginian, Turonian, and Maastrichtian, respectively.

All our estimates for aquifer-eustasy are an order of magnitude below the reported eustatic magnitudes of 65, 30, and 50 m for the Valanginian, Turonian, and Maastrichtian, respectively (Ray et al., 2019). Moreover, even if lakes were able to contribute an additional 2 m eustatic response and different orbital parameters acted to completely move arid areas into ocean basins so that all land areas were humid, the total aquifer-eustasy response would remain less than 5 m. This result casts significant doubt on the role of aquifer-eustasy in controlling Cretaceous short-term cycles. In contrast to the generally held view on Cretaceous aquifer-eustasy, the spatial extent of fully arid land areas increases with higher CO_2 forcing. Therefore, if aquifer-eustasy is an active component of Cretaceous sea level, then lower sea levels should occur during cooler periods in contrast to the current view (Wendler and Wendler, 2016; Sames et al., 2020). This interpretation means glacio-, thermo-, and aquifer-eustasy can work in phase during the Cretaceous, implying that any Cretaceous ice caps inferred to explain the observed sea-level response can be smaller than previously thought. Whilst further work is necessary to assess the impact of lakes and orbital forcing on these estimates and to test our conclusions that aquifer- and glacio-eustasy would be in phase, this research strongly indicates that glacio-eustasy was the main driver of Cretaceous short-term eustatic cycles, supporting the growing body of evidence against ubiquitous Cretaceous warmth.

Acknowledgements

The authors thank Halliburton for permission to publish this paper, Prof. Y. Fan Reinfelder for sharing the data on water table depths. We also thank Andrew Gale and an anonymous reviewer for their thoughtful feedback that helped improve this manuscript, as well as Eduardo Koutsoukos for editorial assistance.

References

Alley, N.F., Hore, S.B., Frakes, L.A., 2019. Glaciations at high-latitude Southern Australia during the Early Cretaceous. Australian Journal of Earth Sciences. https://doi.org/10.1080/08120099.2019.1590457

Barclay, R.S., McElwain, J.C., Sageman, B.B., 2010. Carbon sequestration activated by a volcanic CO 2 pulse during Ocean Anoxic Event 2. Nature Geoscience 3, 205–208. https://doi.org/10.1038/ngeo757

Berg, A., Findell, K., Lintner, B., Giannini, A., Seneviratne, S.I., van den Hurk, B., Lorenz, R., Pitman, A., Hagemann, S., Meier, A., Cheruy, F., Ducharne, A., Malyshev, S., Milly, P.C.D., 2016. Land–atmosphere feedbacks amplify aridity increase over land under global warming. Nature Climate Change 6, 869–874. https://doi.org/10.1038/nclimate3029

Bernard, S., Daval, D., Ackerer, P., Pont, S., Meibom, A., 2017. Burial-induced oxygen-isotope re-equilibration of fossil foraminifera explains ocean paleotemperature paradoxes. Nature Communications 8, 1134. https://doi.org/10.1038/s41467-017-01225-9

Bornemann, A., Norris, R.D., Friedrich, O., Beckmann, B., Schouten, S., Damsté, J.S.S., Vogel, J., Hofmann, P., Wagner, T., 2008. Isotopic Evidence for Glaciation During the Cretaceous Supergreenhouse. Science 319, 189–192. https://doi.org/10.1126/science.1148777

Boucot, A.J., Xu, C., Scotese, C.R., Morley, R.J., 2013. Phanerozoic Paleoclimate: An Atlas of Lithologic Indicators of Climate. SEPM (Society for Sedimentary Geology), Tulsa, Oklahoma, U.S.A. https://doi.org/10.2110/sepmcsp.11

Boulila, S., Galbrun, B., Miller, K.G., Pekar, S.F., Browning, J.V., Laskar, J., Wright, J.D., 2011. On the origin of Cenozoic and Mesozoic “third-order” eustatic sequences. Earth-Science Reviews 109, 94–112. https://doi.org/10.1016/j.earscirev.2011.09.003

Bowman, V.C., Francis, J.E., Askin, R.A., Riding, J.B., Swindles, G.T., 2014. Latest Cretaceous–earliest Paleogene vegetation and climate change at the high southern latitudes: palynological evidence from Seymour Island, Antarctic Peninsula. Palaeogeography, Palaeoclimatology, Palaeoecology 408, 26–47. https://doi.org/10.1016/j.palaeo.2014.04.018

Bowman, V.C., Francis, J.E., Riding, J.B., 2013. Late Cretaceous winter sea ice in Antarctica? Geology 41, 1227–1230. https://doi.org/10.1130/G34891.1

Breecker, D.O., Sharp, Z.D., McFadden, L.D., 2010. Atmospheric CO2 concentrations during ancient greenhouse climates were similar to those predicted for A.D. 2100. Proceedings of the National Academy of Sciences 107, 576–580. https://doi.org/10.1073/pnas.0902323106

Buatois, L.A., Echevarría, C., 2019. Ichnofabrics from a Cretaceous Eolian System of Western Argentina: Expanding the Application of Core Ichnology to Desert Environments. Palaios 34, 190–211. https://doi.org/10.2110/palo.2018.110

Cramer, B.S., Miller, K.G., Barrett, P.J., Wright, J.D., 2011. Late Cretaceous–Neogene trends in deep ocean temperature and continental ice volume: Reconciling records of benthic foraminiferal geochemistry (δ18O and Mg/Ca) with sea level history. Journal of Geophysical Research: Oceans 116. https://doi.org/10.1029/2011JC007255

Dal' Bó, P.F.F., Basilici, G., Angelica, R.S., Ladeira, F.S.B., 2009. Paleoclimatic interpretations from pedogenic calcretes in a Maastrichtian semi-arid eolian sand-sheet palaeoenvironment: Marília Formation (Bauru Basin, southeastern Brazil). Cretaceous Research 30, 659–675. https://doi.org/10.1016/j.cretres.2008.12.006

Davies, A., Hunter, S.J., Gréselle, B., Haywood, A.M., Robson, C., 2019. Evidence for seasonality in early Eocene high latitude sea-surface temperatures. Earth and Planetary Science Letters 519, 274–283. https://doi.org/10.1016/j.epsl.2019.05.025

Davies, A., Kemp, A.E.S., Pike, J., 2009. Late Cretaceous seasonal ocean variability from the Arctic. Nature 460, 254–258. https://doi.org/10.1038/nature08141

Dickie, K., Keen, C.E., Williams, G.L., Dehler, S.A., 2011. Tectonostratigraphic evolution of the Labrador margin, Atlantic Canada. Marine and Petroleum Geology 28, 1663–1675. https://doi.org/10.1016/j.marpetgeo.2011.05.009

Essery, R.L.H., Best, M.J., Betts, R.A., Cox, P.M., Taylor, C.M., 2003. Explicit Representation of Subgrid Heterogeneity in a GCM Land Surface Scheme. J. Hydrometeor. 4, 530–543. https://doi.org/10.1175/1525-7541(2003)004<0530:EROSHI>2.0.CO;2

Fan, Y., Li, H., Miguez-Macho, G., 2013. Global Patterns of Groundwater Table Depth. Science 339, 940–943. https://doi.org/10.1126/science.1229881

Fan, Y., Miguez-Macho, G., Jobbágy, E.G., Jackson, R.B., Otero-Casal, C., 2017. Hydrologic regulation of plant rooting depth. Proc. Natl. Acad. Sci. U.S.A. 114, 10572–10577. https://doi.org/10.1073/pnas.1712381114

Föllmi, K.B., 2012. Early Cretaceous life, climate and anoxia. Cretaceous Research 35, 230–257. https://doi.org/10.1016/j.cretres.2011.12.005

Gale, A.S., Hardenbol, J., Hathway, B., Kennedy, W.J., Young, J.R., Phansalkar, V., 2002. Global correlation of Cenomanian (Upper Cretaceous) sequences: Evidence for Milankovitch control on sea level. Geology 30, 291–294. https://doi.org/10.1130/0091-7613(2002)030<0291:GCOCUC>2.0.CO;2

Galeotti, S., Rusciadelli, G., Sprovieri, M., Lanci, L., Gaudio, A., Pekar, S., 2009. Sea-level control on facies architecture in the Cenomanian–Coniacian Apulian margin (Western Tethys): A record of glacio-eustatic fluctuations during the Cretaceous greenhouse? Palaeogeography, Palaeoclimatology, Palaeoecology 276, 196–205. https://doi.org/10.1016/j.palaeo.2009.03.011

Gordon, C., Cooper, C., Senior, C.A., Banks, H., Gregory, J.M., Johns, T.C., Mitchell, J.F.B., Wood, R.A., 2000. The simulation of SST, sea ice extents and ocean heat transports in a version of the Hadley Centre coupled model without flux adjustments. Climate Dynamics 16, 147–168. https://doi.org/10.1007/s003820050010

Granot, R., Dyment, J., 2015. The Cretaceous opening of the South Atlantic Ocean. Earth and Planetary Science Letters 414, 156–163. https://doi.org/10.1016/j.epsl.2015.01.015

Grasby, S.E., McCune, G.E., Beauchamp, B., Galloway, J.M., 2017. Lower Cretaceous cold snaps led to widespread glendonite occurrences in the Sverdrup Basin, Canadian High Arctic. GSA Bulletin 129, 771–787. https://doi.org/10.1130/B31600.1

Gréselle, B., Pittet, B., 2010. Sea-level reconstructions from the Peri-Vocontian Zone (South-east France) point to Valanginian glacio-eustasy. Sedimentology 57, 1640–1684. https://doi.org/10.1111/j.1365-3091.2010.01159.x

Haq, B.U., 2014. Cretaceous eustasy revisited. Global and Planetary Change 113, 44–58. https://doi.org/10.1016/j.gloplacha.2013.12.007

Haq, B.U., Huber, B.T., 2017. Anatomy of a eustatic event during the Turonian (Late Cretaceous) hot greenhouse climate. Sci. China Earth Sci. 60, 20–29. https://doi.org/10.1007/s11430-016-0166-y

Hasegawa, H., Tada, R., Jiang, X., Suganuma, Y., Imsamut, S., Charusiri, P., Ichinnorov, N., Khand, Y., 2012. Drastic shrinking of the Hadley circulation during the mid-Cretaceous Supergreenhouse. Climate of the Past 8, 1323–1337. https://doi.org/10.5194/cp-8-1323-2012

Hay, W.W., DeConto, R.M., Boer, P. de, Flögel, S., Song, Y., Stepashko, A., 2019. Possible solutions to several enigmas of Cretaceous climate. Int J Earth Sci (Geol Rundsch) 108, 587–620. https://doi.org/10.1007/s00531-018-1670-2

Hay, W.W., Floegel, S., 2012. New thoughts about the Cretaceous climate and oceans. Earth-Science Reviews 115, 262–272. https://doi.org/10.1016/j.earscirev.2012.09.008

Hay, W.W., Leslie, M.A., 1990. Could Possible Changes in Global Groundwater Reservoir Cause Eustatic Sea-Level Fluctuations?, in: Sea-Level Change: Studies in Geophysics. The National Academies Press, pp. 161–170. https://doi.org/10.17226/1345

Ho, S.L., Laepple, T., 2016. Flat meridional temperature gradient in the early Eocene in the subsurface rather than surface ocean. Nature Geoscience 9, 606–610. https://doi.org/10.1038/ngeo2763

Hollis, C.J., Taylor, K.W.R., Handley, L., Pancost, R.D., Huber, M., Creech, J.B., Hines, B.R., Crouch, E.M., Morgans, H.E.G., Crampton, J.S., Gibbs, S., Pearson, P.N., Zachos, J.C., 2012. Early Paleogene temperature history of the Southwest Pacific Ocean: Reconciling proxies and models. Earth and Planetary Science Letters 349–350, 53–66. https://doi.org/10.1016/j.epsl.2012.06.024

Huang, J., Ji, M., Xie, Y., Wang, S., He, Y., Ran, J., 2016. Global semi-arid climate change over last 60 years. Clim Dyn 46, 1131–1150. https://doi.org/10.1007/s00382-015-2636-8

Huber, B.T., Norris, R.D., MacLeod, K.G., 2002. Deep-sea paleotemperature record of extreme warmth during the Cretaceous. Geology 30, 123–126. https://doi.org/10.1130/0091-7613(2002)030<0123:DSPROE>2.0.CO;2

Immenhauser, A., 2005. High-rate sea-level change during the Mesozoic: New approaches to an old problem. Sedimentary Geology, Sedimentology in the 21st Century - A Tribute to Wolfgang Schlager 175, 277–296. https://doi.org/10.1016/j.sedgeo.2004.12.016

Jacobs, D.K., Sahagian, D.L., 1993. Climate-induced fluctuations in sea level during non-glacial times. Nature 361, 710–712. https://doi.org/10.1038/361710a0

Jarvis, I., Lignum, J.S., Gröcke, D.R., Jenkyns, H.C., Pearce, M.A., 2011. Black shale deposition, atmospheric CO2 drawdown, and cooling during the Cenomanian-Turonian Oceanic Anoxic Event. Paleoceanography 26, PA3201. https://doi.org/10.1029/2010PA002081

Jarvis, I., Trabucho-Alexandre, J., Gröcke, D.R., Uličný, D., Laurin, J., 2015. Intercontinental correlation of organic carbon and carbonate stable isotope records: evidence of climate and sea-level change during the Turonian (Cretaceous). The Depositional Record 1, 53–90. https://doi.org/10.1002/dep2.6

Jenkyns, H.C., Forster, A., Schouten, S., Damsté, J.S.S., 2004. High temperatures in the Late Cretaceous Arctic Ocean. Nature 432, 888–892. https://doi.org/10.1038/nature03143

Kindler, P., Davaud, E., 2001. Recognizing Eolianites in thin Section. Review and Case Study—the Lower Cretaceous Chambotte Formation, SalÈVe Chain, Southeastern France, in: (Rick) Abegg, F.E., (Mitch) Harris, P.M., Loope, D.B. (Eds.), Modern and Ancient Carbonate Eolianites: Sedimentology, Sequence Stratigraphy, and Diagenesis, SEPM Special Publication. SEPM (Society for Sedimentary Geology), pp. 141–150. https://doi.org/10.2110/pec.01.71.0141

Koch, J.T., Brenner, R.L., 2009. Evidence for glacioeustatic control of large, rapid sea-level fluctuations during the Albian-Cenomanian: Dakota formation, eastern margin of western interior seaway, USA. Cretaceous Research 30, 411–423. https://doi.org/10.1016/j.cretres.2008.08.002

Kominz, M.A., Browning, J.V., Miller, K.G., Sugarman, P.J., Mizintseva, S., Scotese, C.R., 2008. Late Cretaceous to Miocene sea-level estimates from the New Jersey and Delaware coastal plain coreholes: an error analysis. Basin Research 20, 211–226. https://doi.org/10.1111/j.1365-2117.2008.00354.x

Kontorovich, A.E., Ershov, S.V., Kazanenkov, V.A., Karogodin, Yu.N., Kontorovich, V.A., Lebedeva, N.K., Nikitenko, B.L., Popova, N.I., Shurygin, B.N., 2014. Cretaceous paleogeography of the West Siberian sedimentary basin. Russian Geology and Geophysics, Urgent Problems of Petroleum Geology (dedicated to the 80th birthday of Academician Aleksei E. Kontorovich) 55, 582–609. https://doi.org/10.1016/j.rgg.2014.05.005

Kottek, M., Grieser, J., Beck, C., Rudolf, B., Rubel, F., 2006. World Map of the Köppen-Geiger climate classification updated. Meteorologische Zeitschrift 259–263. https://doi.org/10.1127/0941-2948/2006/0130

Ladant, J.-B., Donnadieu, Y., 2016. Palaeogeographic regulation of glacial events during the Cretaceous supergreenhouse. Nature Communications 7, 1–9. https://doi.org/10.1038/ncomms12771

Laurin, J., Barclay, R.S., Sageman, B.B., Dawson, R.R., Pagani, M., Schmitz, M., Eaton, J., McInerney, F.A., McElwain, J.C., 2019. Terrestrial and marginal-marine record of the mid-Cretaceous Oceanic Anoxic Event 2 (OAE 2): High-resolution framework, carbon isotopes, CO2 and sea-level change. Palaeogeography, Palaeoclimatology, Palaeoecology 524, 118–136. https://doi.org/10.1016/j.palaeo.2019.03.019

Lin, W., Bhattacharya, J.P., Stockford, A., 2019. High-resolution Sequence Stratigraphy and Implications For Cretaceous Glacioeustasy of the Late Cretaceous Gallup System, New Mexico, U.S.A. Journal of Sedimentary Research 89, 552–575. https://doi.org/10.2110/jsr.2019.32

Macquaker, J.H.S., Keller, M.A., 2005. Mudstone Sedimentation at High Latitudes: Ice as a Transport Medium for Mud and Supplier of Nutrients. Journal of Sedimentary Research 75, 696–709. https://doi.org/10.2110/jsr.2005.056

Mannion, P.D., Benson, R.B.J., Carrano, M.T., Tennant, J.P., Judd, J., Butler, R.J., 2015. Climate constrains the evolutionary history and biodiversity of crocodylians. Nature Communication 6, 1–9. https://doi.org/10.1038/ncomms9438

Maurer, F., Buchem, F.S.P. van, Eberli, G.P., Pierson, B.J., Raven, M.J., Larsen, P.-H., Al-Husseini, M.I., Vincent, B., 2013. Late Aptian long-lived glacio-eustatic lowstand recorded on the Arabian Plate. Terra Nova 25, 87–94. https://doi.org/10.1111/ter.12009

McAnena, A., Flögel, S., Hofmann, P., Herrle, J.O., Griesand, A., Pross, J., Talbot, H.M., Rethemeyer, J., Wallmann, K., Wagner, T., 2013. Atlantic cooling associated with a marine biotic crisis during the mid-Cretaceous period. Nature Geosci 6, 558–561. https://doi.org/10.1038/ngeo1850

Miall, A.D., Catuneanu, O., 2019. Chapter 9 - The Western Interior Basin, in: Miall, A.D. (Ed.), The Sedimentary Basins of the United States and Canada (Second Edition). Elsevier, pp. 401–443. https://doi.org/10.1016/B978-0-444-63895-3.00009-7

Miller, K.G., Kominz, M.A., Browning, J.V., Wright, J.D., Mountain, G.S., Katz, M.E., Sugarman, P.J., Cramer, B.S., Christie-Blick, N., Pekar, S.F., 2005a. The Phanerozoic Record of Global Sea-Level Change. Science 310, 1293–1298. https://doi.org/10.1126/science.1116412

Miller, K.G., Wright, J.D., Browning, J.V., 2005b. Visions of ice sheets in a greenhouse world. Marine Geology, Ocean Chemistry over the Phanerozoic and its links to Geological Processes 217, 215–231. https://doi.org/10.1016/j.margeo.2005.02.007

Mountney, N., Howell, J., Flint, S., Jerram, D., 1998. Aeolian and alluvial deposition within the Mesozoic Etjo Sandstone Formation, northwest Namibia. Journal of African Earth Sciences 27, 175–192. https://doi.org/10.1016/S0899-5362(98)00056-6

Mutterlose, J., Bornemann, A., Herrle, J., 2009. The Aptian Albian cold snap: Evidence for "mid" Cretaceous icehouse interludes. Neues Jahrbuch für Geologie und Paläontologie - Abhandlungen 252, 217–225. https://doi.org/10.1127/0077-7749/2009/0252-0217

Niezgodzki, I., Tyszka, J., Knorr, G., Lohmann, G., 2019. Was the Arctic Ocean ice free during the latest Cretaceous? The role of CO2 and gateway configurations. Global and Planetary Change 177, 201–212. https://doi.org/10.1016/j.gloplacha.2019.03.011

O'Brien, C.L., Robinson, S.A., Pancost, R.D., Sinninghe Damsté, J.S., Schouten, S., Lunt, D.J., Alsenz, H., Bornemann, A., Bottini, C., Brassell, S.C., Farnsworth, A., Forster, A., Huber, B.T., Inglis, G.N., Jenkyns, H.C., Linnert, C., Littler, K., Markwick, P., McAnena, A., Mutterlose, J., Naafs, B.D.A., Püttmann, W., Sluijs, A., van Helmond, N.A.G.M., Vellekoop, J., Wagner, T., Wrobel, N.E., 2017. Cretaceous sea-surface temperature evolution: Constraints from TEX86 and planktonic foraminiferal oxygen isotopes. Earth-Science Reviews 172, 224–247. https://doi.org/10.1016/j.earscirev.2017.07.012

Pope, V.D., Gallani, M.L., Rowntree, P.R., Stratton, R.A., 2000. The impact of new physical parametrizations in the Hadley Centre climate model: HadAM3. Climate Dynamics 16, 123–146. https://doi.org/10.1007/s003820050009

Pucéat, E., Lécuyer, C., Sheppard, S.M.F., Dromart, G., Reboulet, S., Grandjean, P., 2003. Thermal evolution of Cretaceous Tethyan marine waters inferred from oxygen isotope composition of fish tooth enamels. Paleoceanography 18, 1029. https://doi.org/10.1029/2002PA000823

Ray, D.C., van Buchem, F.S.P., Baines, G., Davies, A., Gréselle, B., Simmons, M.D., Robson, C., 2019. The magnitude and cause of short-term eustatic Cretaceous sea-level change: A synthesis. Earth-Science Reviews 197, 102901. https://doi.org/10.1016/j.earscirev.2019.102901

Reichgelt, T., West, C.K., Greenwood, D.R., 2018. The relation between global palm distribution and climate. Sci Rep 8, 1–11. https://doi.org/10.1038/s41598-018-23147-2

Rubel, F., Kottek, M., 2010. Observed and projected climate shifts 1901-2100 depicted by world maps of the Köppen-Geiger climate classification. Meteorologische Zeitschrift 19, 135–141. https://doi.org/10.1127/0941-2948/2010/0430

Sames, B., Wagreich, M., Conrad, C.P., Iqbal, S., 2020. Aquifer-eustasy as the main driver of short-term sea-level fluctuations during Cretaceous hothouse climate phases. Geological Society, London, Special Publications 498. https://doi.org/10.1144/SP498-2019-105

Sames, B., Wagreich, M., Wendler, J.E., Haq, B.U., Conrad, C.P., Melinte-Dobrinescu, M.C., Hu, X., Wendler, I., Wolfgring, E., Yilmaz, I.Ö., Zorina, S.O., 2016. Review: Short-term sea-level changes in a greenhouse world — A view from the Cretaceous. Palaeogeography, Palaeoclimatology, Palaeoecology, Advances and Perspectives in Understanding Cretaceous Sea-level Change 441, 393–411. https://doi.org/10.1016/j.palaeo.2015.10.045

Scherer, C.M.S., 2002. Preservation of aeolian genetic units by lava flows in the Lower Cretaceous of the Paraná Basin, southern Brazil. Sedimentology 49, 97–116. https://doi.org/10.1046/j.1365-3091.2002.00434.x

Sundquist, E.T., 1990. Long-term aspects of future atmospheric CO2 and sea-level changes, in: Revelle, R. (Ed.), Sea-Level Change. National Academy Press, pp. 193–207.

Totterdell, J.M., Cook, P.J., Bradshaw, M.T., Wilford, G.E., Yeates, A.N., Yeung, M., Truswell, E.M., Brakel, A.T., Isem, A.R., Olissoff, S., Strusz, D.L., Langford, R.P., 2001. Palaeogeographic Atlas of Australia (a set of ten volumes) [WWW Document]. URL http://pid.geoscience.gov.au/dataset/ga/35880

Uličný, D., Jarvis, I., Gröcke, D.R., Čech, S., Laurin, J., Olde, K., Trabucho-Alexandre, J., Švábenická, L., Pedentchouk, N., 2014. A high-resolution carbon-isotope record of the Turonian stage correlated to a siliciclastic basin fill: Implications for mid-

Cretaceous sea-level change. Palaeogeography, Palaeoclimatology, Palaeoecology 405, 42–58. https://doi.org/10.1016/j.palaeo.2014.03.033

Vandermark, D., Tarduno, J.A., Brinkman, D.B., 2007. A fossil champsosaur population from the high Arctic: Implications for Late Cretaceous paleotemperatures. Palaeogeography, Palaeoclimatology, Palaeoecology 248, 49–59. https://doi.org/10.1016/j.palaeo.2006.11.008

Vérard, C., Hochard, C., Baumgartner, P.O., Stampfli, G.M., Liu, M., 2015. 3D palaeogeographic reconstructions of the Phanerozoic versus sea-level and Sr-ratio variations. Journal of Palaeogeography 4, 64–84. https://doi.org/10.3724/SP.J.1261.2015.00068

Vickers, M.L., Price, G.D., Jerrett, R.M., Sutton, P., Watkinson, M.P., FitzPatrick, M., 2019. The duration and magnitude of Cretaceous cool events: Evidence from the northern high latitudes. GSA Bulletin 131, 1979–1994. https://doi.org/10.1130/B35074.1

Voigt, S., Gale, A.S., Voigt, T., 2006. Sea-level change, carbon cycling and palaeoclimate during the Late Cenomanian of northwest Europe; an integrated palaeoenvironmental analysis. Cretaceous Research 27, 836–858. https://doi.org/10.1016/j.cretres.2006.04.005

Wagreich, M., Lein, R., Sames, B., 2014. Eustasy, its controlling factors, and the limno-eustatic hypothesis – concepts inspired by Eduard Suess 107, 115–13117.

Wagreich, M., Sames, B., Hart, M., Yilmaz, I.O., 2020. An Introduction to Causes and Consequences of Cretaceous Sea-Level Changes (IGCP 609). Geological Society, London, Special Publications 498. https://doi.org/10.1144/SP498-2019-156

Wang, Y., Huang, C., Sun, B., Quan, C., Wu, J., Lin, Z., 2014. Paleo-CO2 variation trends and the Cretaceous greenhouse climate. Earth-Science Reviews 129, 136–147. https://doi.org/10.1016/j.earscirev.2013.11.001

Wendler, J.E., Meyers, S.R., Wendler, I., Kuss, J., 2014. A million-year-scale astronomical control on Late Cretaceous sea-level. Newsletters on Stratigraphy 47, 1–19. https://doi.org/10.1127/0078-0421/2014/0038

Wendler, J.E., Wendler, I., 2016. What drove sea-level fluctuations during the mid-Cretaceous greenhouse climate? Palaeogeography, Palaeoclimatology, Palaeoecology, Advances and Perspectives in Understanding Cretaceous Sea-level Change 441, 412–419. https://doi.org/10.1016/j.palaeo.2015.08.029

Wendler, J.E., Wendler, I., Vogt, C., Kuss, J., 2016. Link between cyclic eustatic sea-level change and continental weathering: Evidence for aquifer-eustasy in the Cretaceous. Palaeogeography, Palaeoclimatology, Palaeoecology, Advances and Perspectives in Understanding Cretaceous Sea-level Change 441, 430–437. https://doi.org/10.1016/j.palaeo.2015.08.014

Wilmsen, M., Nagm, E., 2013. Sequence stratigraphy of the lower Upper Cretaceous (Upper Cenomanian - Turonian) of the Eastern Desert, Egypt. Newsletters on Stratigraphy 46, 23–46. https://doi.org/10.1127/0078-0421/2013/0030

Figures

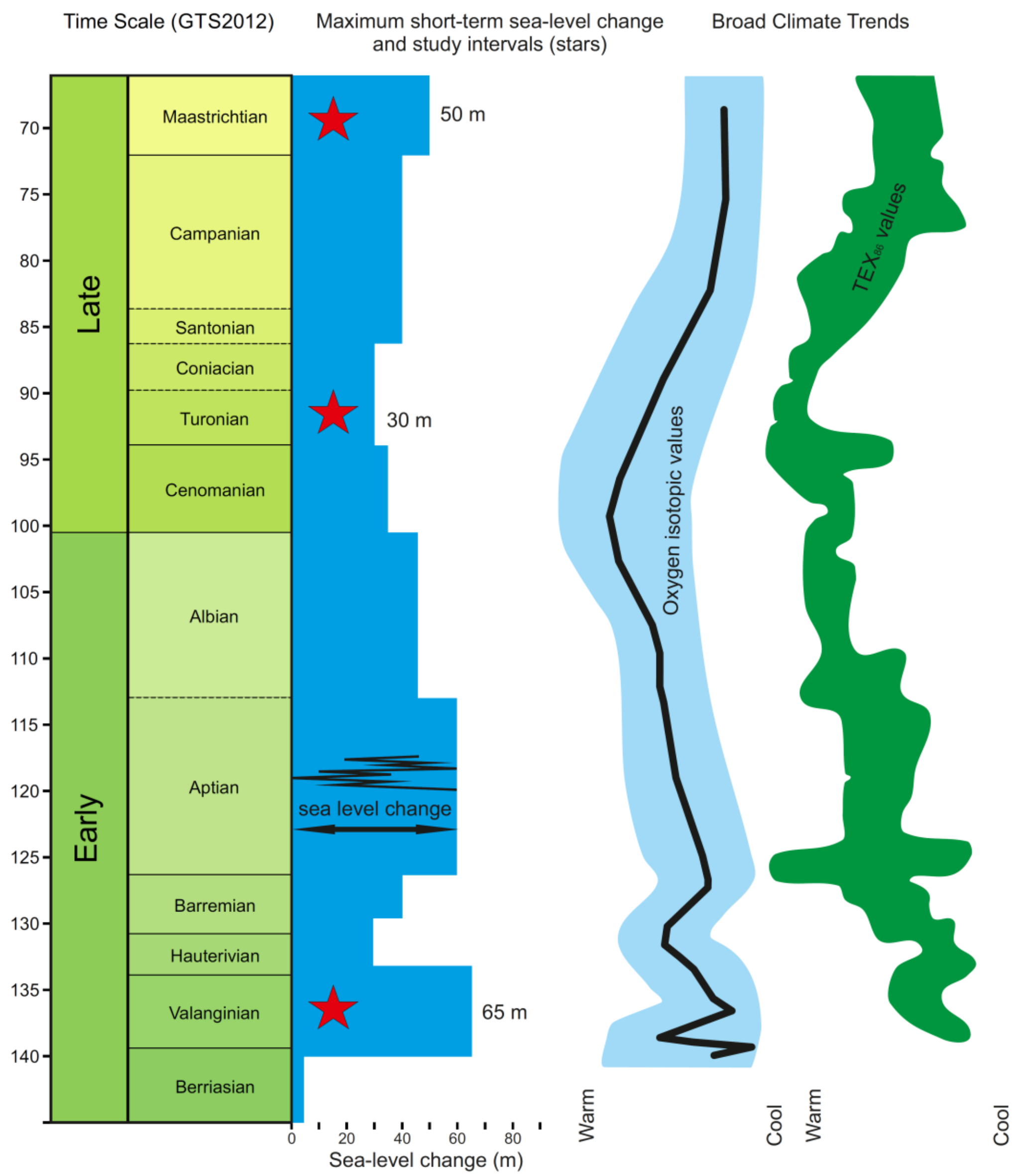

Figure 1. Maximum short-term magnitude of sea-level change (Ray et al. 2019), the chronostratigraphic location of the study intervals, and broad Cretaceous climate proxies [oxygen isotopic variations in fish teeth from the western Tethys from Pucéat et al. (2003) and the TEX_{86} compilation of O'Brien et al. (2017)]. Figure modified from Ray et al. (2019).

Time interval	Low CO_2	Medium CO_2	High CO_2
Maastrichtian	409	810	1379
Turonian	907	1300	1850
Valanginian	650	1087	1540

Table 1. CO_2 values used for the nine simulations.

Time period	Global mean precipitation over land (mm/day)		
	Low CO_2	Medium CO_2	High CO_2
Maastrichtian	2.27	2.46	2.69
Turonian	2.45	2.54	2.66
Valanginian	1.99	2.00	1.96

Table 2. Mean global precipitation over land for the different simulations, accounting for the differing zonal areal extent with latitude.

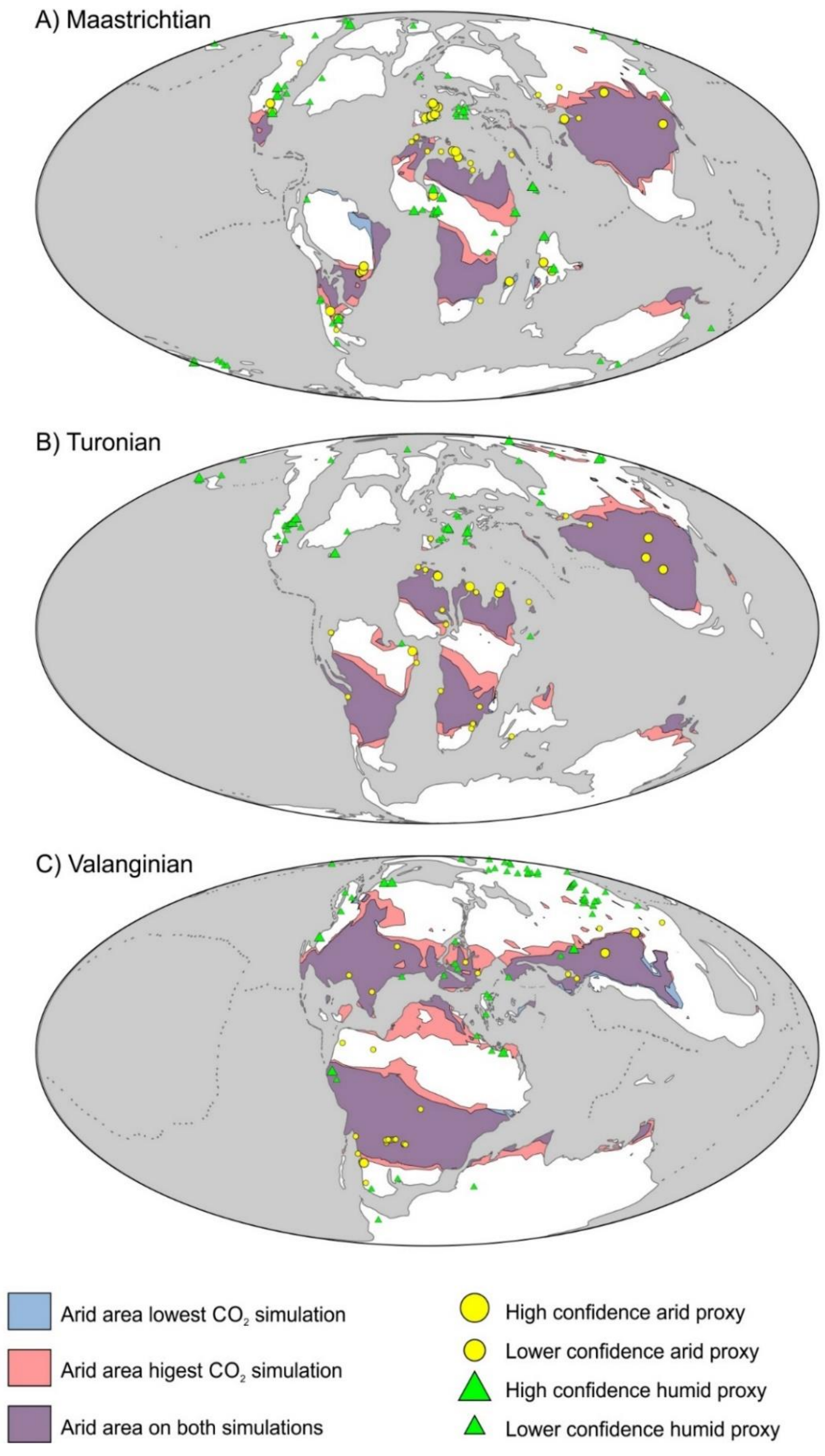

Figure 2. Simulated extent of fully arid land area on the lowest (blue) and highest CO_2 simulations (red) for the Maastrichtian (A), Turonian (B), and Valanginian (C). Areas that are

fully humid under both CO_2 forcing are in purple. Proxy data control for humid and arid environments are also depicted.

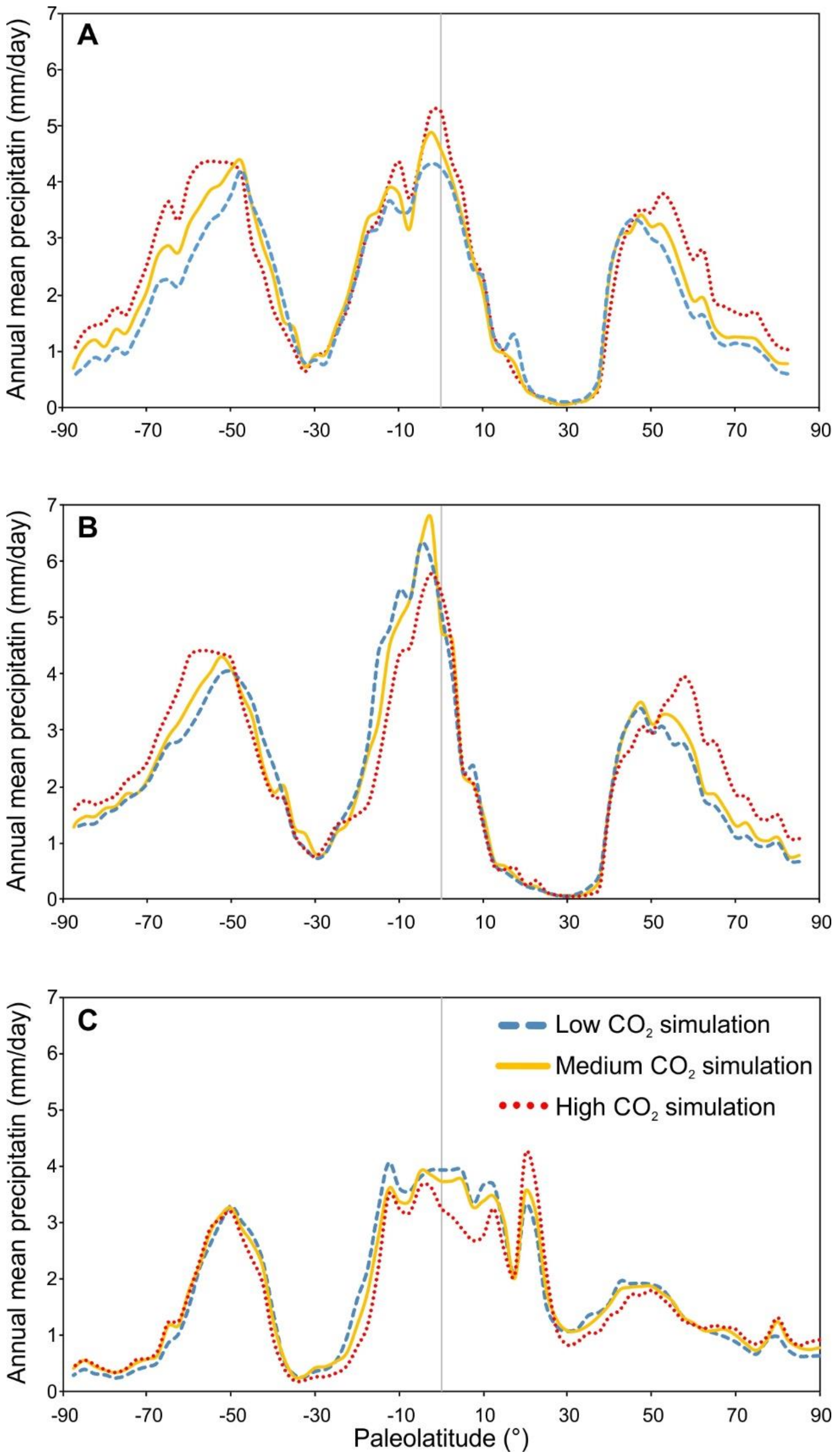

745

746 Figure 3. Zonal median annual precipitation for the low, medium, and high CO_2 forcing for

747 the Maastrichtian (A), Turonian (B), and Valanginian (C).

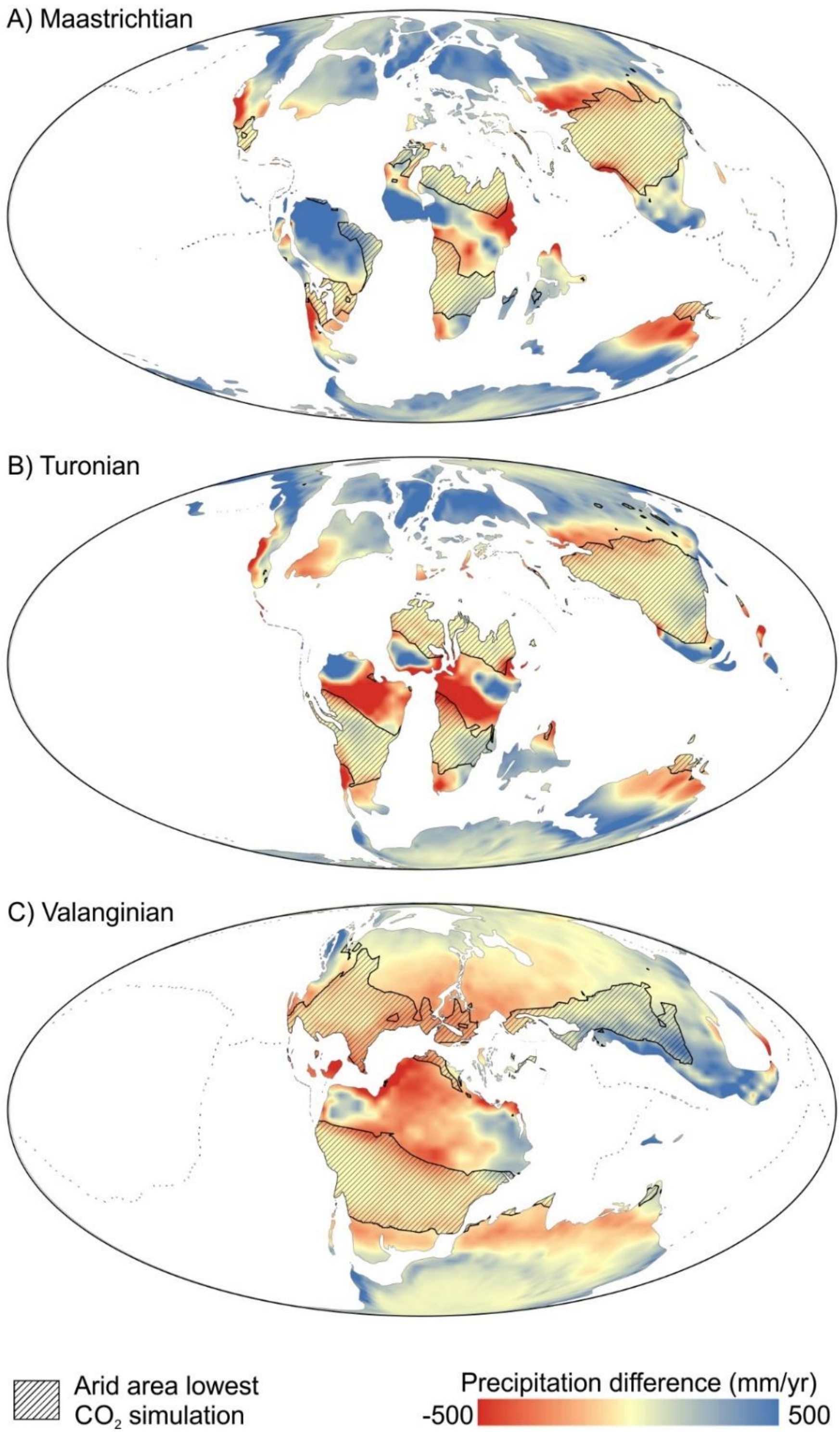

Figure 4. Difference in precipitation between the simulations with the highest and lowest atmospheric CO_2 concentrations for the Maastrichtian (A), Turonian (B), and Valanginian (C). Negative values indicate lower precipitation in the highest CO_2 simulation, and blue reflects higher precipitation in the highest CO_2 simulation. The fully arid land area on the lowest CO_2 simulation is also shown.

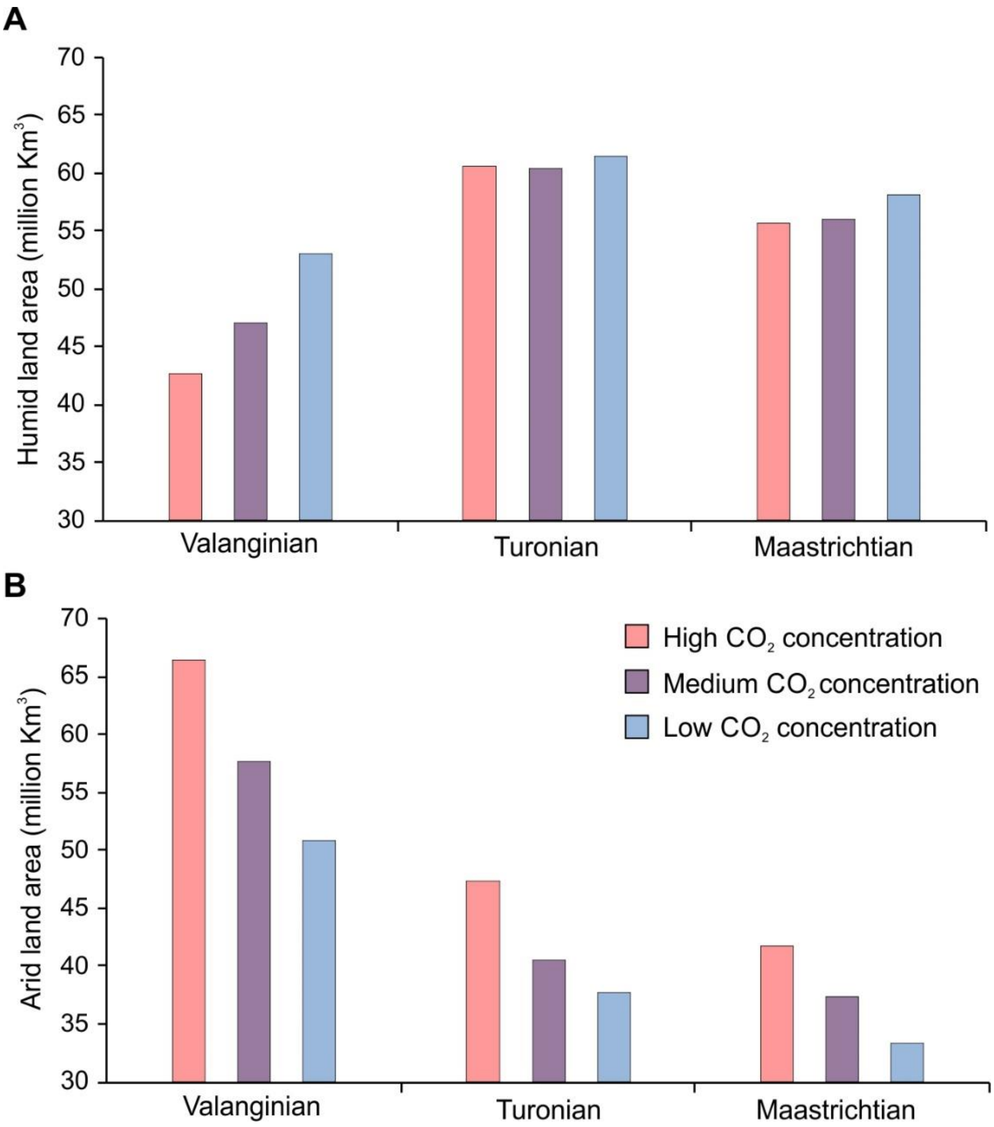

Figure 5. Areal extent of fully humid (A) and fully arid (B) land area for the high, medium, and low simulations for each time slice. The fully arid land area demonstrates a consistent reduction in size with lower atmospheric CO_2 concentrations. Lower CO_2 concentrations generally equate to a larger humid land area, although, apart from the Valanginian, the differences are more muted.

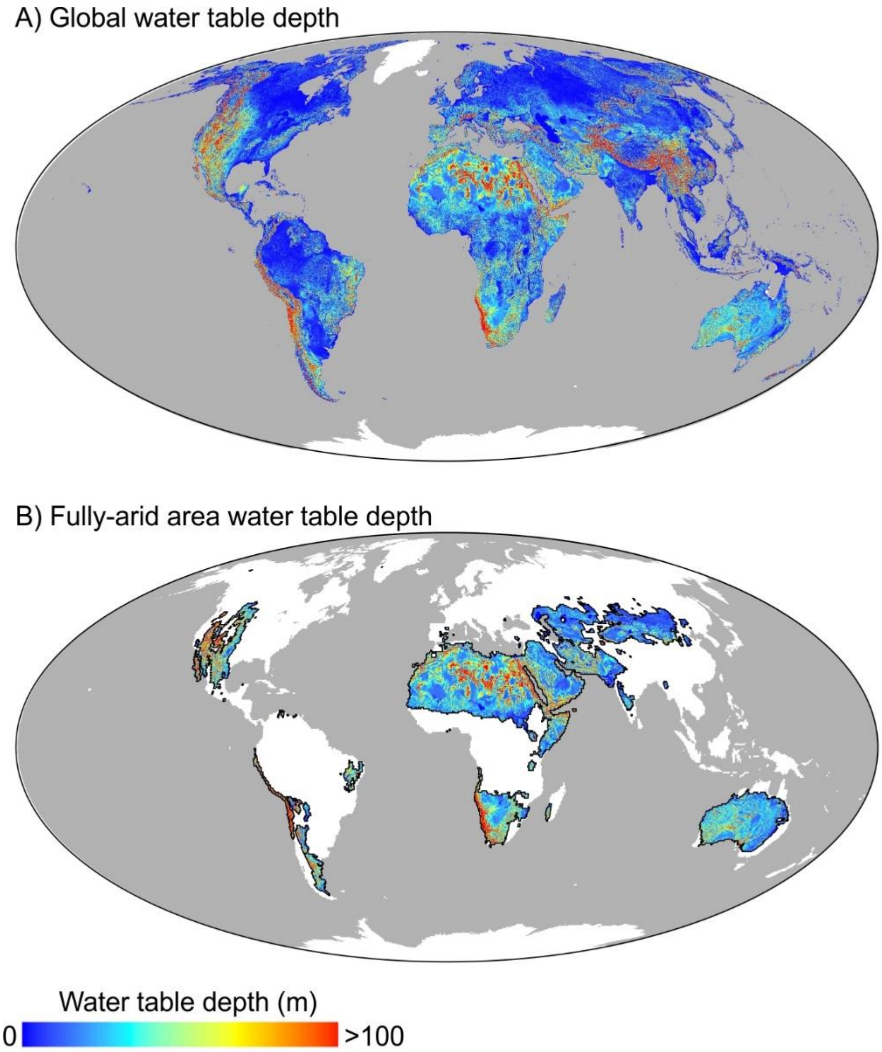

Figure 6. Modern water table depth from Fan et al. (2017), and an extraction for the fully arid land area using the Köppen-Geiger map for 1976-2000 from Rubel and Kottek (2010).

Time period	Scenario	Land area ($x10^6$ km^2)	Volume of water ($x10^6$ km^3)	Eustatic response (m)	Eustatic estimate (m)*
Maastrichtian	1	8.4	0.03	0.10	~50
	2	37.3	0.15	0.44	
	3	135.8	1.06	1.82	
Turonian	1	9.6	0.04	0.11	~30
	2	40.6	0.17	0.48	
	3	136.7	1.07	1.83	
Valanginian	1	15.6	0.06	0.21	~65
	2	57.6	0.24	0.78	
	3	184.4	1.44	2.84	

Table 3. Assuming 30% porosity and 325.6, 373.3, and 374.3 km^3 of water to generate a 1 mm sea-level rise for the Valanginian, Turonian, and Maastrichtian, respectively. In scenario 1 (most likely), we use the change in arid land area and assume a change of water table from the median arid area depth of 25.87 m to the non-arid area median water table depth of 11.20 m; for scenario 2 (unlikely) we use the total arid land area and assume the same water table depths as scenario 1; for scenario 3 (very unlikely) we use the total global land area and assume a change from the global median water table depth of 16.70 to 0 m. *The eustatic estimates are from Ray et al. (2019).

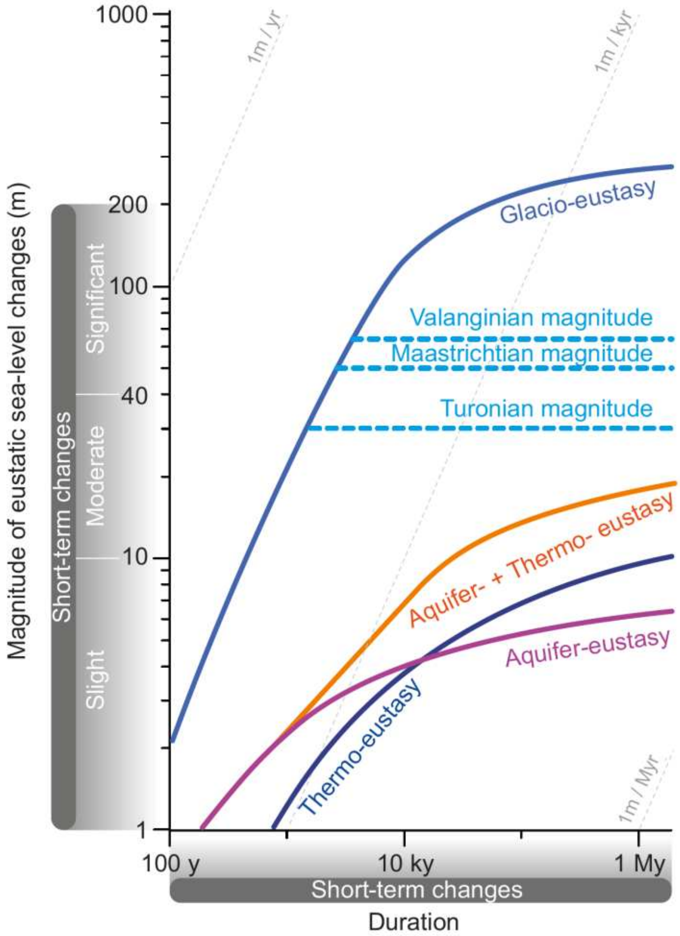

Figure 7. Schematic representation of the duration, magnitude, and rate of known drivers of short-term eustasy, with the upper magnitude limits for Valanginian, Turonian, and Maastrichtian short-term sea-level changes shown (Ray et al. 2019). The curves reflect the upper limits of durations, magnitudes, and rates that are reflective of the climatic drivers of the eustasy [modified from Fig. 7 of Ray et al. (2019)]. Note that even under the most optimistic scenario, the combined eustatic impact of thermo- and aquifer-eustasy is insufficient to account for the reported upper magnitude limits for Valanginian, Turonian, and Maastrichtian.